Journal of Sound and Vibration (1995) **182**(2), 303–322

DYNAMIC ANALYSIS OF A REVERSE-IDLER GEAR PAIR WITH CONCURRENT CLEARANCES

T. E. Rook and R. Singh

Acoustics & Dynamics Laboratory, *Department of Mechanical Engineering*, *The Ohio State University*, *Columbus*, *Ohio* 43210–1107, *U.S.A.*

(*Received* 28 *May* 1993, *and in final form* 7 *March* 1994)

Concurrent non-linearities may be defined as multiple local non-linearities which are linked kinematically to an inertial body in a multi-degree-of-freedom mechanical system. A practical example is found in the reverse-idler gear system which may rattle or undergo vibro-impacts under very light mean loads. Since very little is known about such torsional systems with two or more clearances, an analytical investigation has been undertaken to gain a better understanding of the resulting non-linear behavior. New coupling and scaling procedures are developed to reduce computational difficulties. In an attempt to quantify the average impact behavior in the concurrent gear meshes, the concept of effective stiffness is introduced and calculated from the non-linear response in seveal ways. Response-variant natural frequencies obtained from these effective stiffnesses are then used to study the spectral interaction in a system in which two non-linearities are present simultaneously. Results of the Galerkin method (multi-term harmonic balance) match well with predictions of the numerical integration techniques. Both methods are used to study periodic responses, while the Floquet theory is used to study the stability of such solutions. Techniques for embedding the concept of effective stiffness into each method are also examined. Although the emphasis is on periodic steady state solutions, quasi-periodic responses have been briefly examined due to their prevalence in a system with concurrent nonlinearities.

1. INTRODUCTION

Non-linear dynamic analysis of a MDOF system with one or more clearances has been the subject of several recent investigations [1–4]. Such problems are typically encountered in geared systems, particularly with regards to the rattle phenomenon [5–9]. A typical automotive neutral gear rattle model contains a multi-staged clutch and at least one gear pair with backlash [10, 11]; bearing clearances and spline/synchronizer backlash may also be included. Spectral interactions induced by these non-linear elements have been studied for a simple problem [12]. It has also been seen that numerical solutions may be difficult to obtain under certain circumstances such as when spectral interactions are strong or when both mean load and system damping are very low [1, 10, 12].

In this area several research issues remain unresolved. For instance, dynamic interactions between multiple gear backlashes are yet to be studied. This situation may arise in an automotive transmission when four or five gear pairs along with several synchronizer splines are present. Moreover, backlash is bound to exist in each gear or spline mesh. Yet another problem is the study of reverse-idler gear pairs which may contribute to the rattle phenomena. Such gear pairs are expected to execute conjugate motions under heavy loads but under very light loads they may exhibit complex non-linear responses. Experimental data which may explain this phenomenon are not available, since measurements are typically made for the entire transmission. Nonetheless, it is believed that understanding

0022–460X/95/170303 + 20 $08.00/0

of the multi-mesh rattle problem is particularly important in ensuring a rattle-free transmission [7, 13]. An extensive review of the literature reveals that this issue has not been addressed by many prior researchers [7], although numerous gear dynamic models have been proposed over the past few decades [14]. Literature on the multi-mesh geared systems is sparse and virtually non-existent, especially when various non-linearities are included simultaneously [7, 15]. Accordingly, non-linear dynamic analysis of a generic reverse-idler geared system is chosen as the focus of this investigation, with an emphasis on periodic solutions.

2. PROBLEM FORMULATION

2.1. PHYSICAL SYSTEM

The example case is comprised of the reverse-idler gear pair alone and its lumped parameter torsional model is depicted in Figure 1. The translational degrees of freedom associated with the rolling element bearings and shaft deflections are not considered in this study, and consequently only the external pulsating torque, $T(t)$, rather than the static transmission error [1, 14] is considered as the sole excitation; this excitation is normally applied on the middle gear (B), although it may also be applied to gears A or C. Additionally, the gear mesh stiffnesses, K, are assumed to be time-invariant nominal values, while the dissipation is assumed to be a combination of viscous, C, and impact damping elements.

The backlash non-linearity with impact damping via the empirical parameter β [16], as shown in Figure 1(b), is describe as follows (refer to Appendix A for the identification of symbols):

$$f_i(q_i, \dot{q}_i) = (q_i + (|q_i - b_i| - |q_i + b_i|)/2)(1 + \beta_i \dot{q}_i), \qquad i = 1, 2. \tag{1}$$

2.2. LINEAR SYSTEM

Before studying the non-linear behavior of the physical system shown in Figure 1(a), we will investigate the linear behavior by setting $f_i(q_i, \dot{q}_i) \equiv q_i$. We assume that the viscous

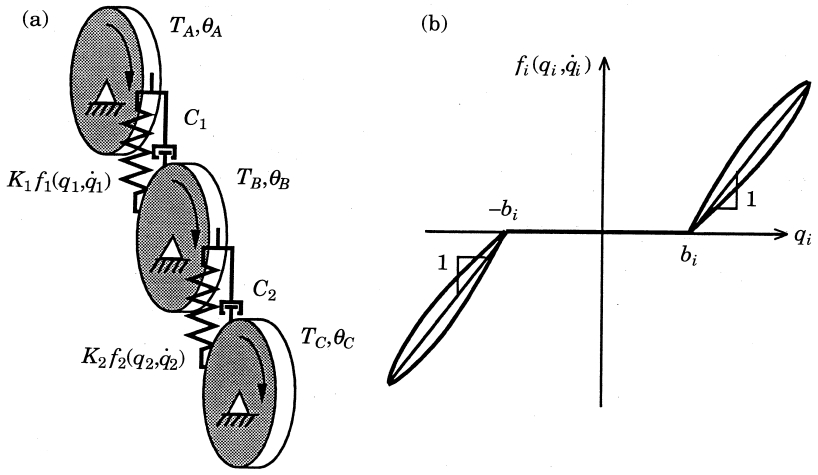

Figure 1. An example case: (a) A schematic of the reverse-idler gear pair, (b) backlash non-linearity with impact damping.

damping ratios for all of the modes are equal to ζ. The uncoupled equations of motion for a linear time-invariant (LTI) system in matrix form become

$$\mathbf{M}\ddot{\mathbf{z}}(t) + \mathbf{C}\dot{\mathbf{z}}(t) + \mathbf{K}\mathbf{z}(t) = \mathbf{F}(t), \tag{2}$$

where the system matrices and vectors are given as follows:

$$\mathbf{z}(t) = \{R_A\theta_A(t) \quad R_B\theta_B(t) \quad R_C\theta_C(t)\}^{\mathrm{T}}, \qquad \mathbf{F}(t) = \{T_A(t)/R_A \quad T_B(t)/R_B \quad T_C(t)/R_C\}^{\mathrm{T}},$$

$$\mathbf{M} = \mathrm{diag}\,(I_A/R_A^2 \quad I_B/R_B^2 \quad I_C/R_C^2), \qquad \mathbf{K} = \begin{bmatrix} K_1 & K_1 & 0 \\ K_1 & (K_1 + K_2) & K_2 \\ 0 & K_2 & K_2 \end{bmatrix}. \tag{3a–d}$$

The excitations are assumed to be expressed as Fourier series, and in practice the time-dependent excitation is applied on only one of the inertia elements. The viscous damping matrix is defined as $\mathbf{C} = 2\zeta(\mathbf{U}\mathbf{\Lambda}^{1/2}\mathbf{U}^{\mathrm{T}})$, where the normal modal matrix $\mathbf{U}$ satisfies $\mathbf{U}^{\mathrm{T}}\mathbf{M}\mathbf{U} = \mathbf{I}$, and $\mathbf{U}^{\mathrm{T}}\mathbf{K}\mathbf{U} = \mathbf{\Lambda}$.

2.3. NON-LINEAR SYSTEM

Equation (2) may then be written in terms of coupled variables and non-dimensionalized. Since we are only interested in the relative displacements q_i in the meshes, coupling the system allows us to reduce the order of the system by one; the coupling eliminates the rigid body mode but leaves the dynamics otherwise unaltered. Coupling of the variables is also helpful in reducing numerical difficulties. Non-dimensionalizing the system with the proper characteristic values helps scale the problem which eliminates some of the numerical difficulties associated with ill-conditioning [12, 17, 18]. The new system of equations becomes

$$\mathbf{I}\mathbf{q}''(\tau) + \tilde{\Omega}^{-1}\mathbf{\Xi}\mathbf{q}'(\tau) + \tilde{\Omega}^{-2}\mathbf{\Gamma}\mathbf{f}(\mathbf{q}(\tau), \mathbf{q}'(\tau)) = \tilde{\Omega}^{-2}\mathbf{Q}(\tau),$$

$$\mathbf{q}(\tau) = \mathbf{P}\mathbf{z}(\tau), \qquad \mathbf{Q}(\tau) = \mathbf{P}\mathbf{M}^{-1}\mathbf{F}(\tau),$$

$$\mathbf{\Gamma} = \omega^{-2}\mathbf{P}\mathbf{M}^{-1}\mathbf{K}\mathbf{P}^{+}, \qquad \mathbf{\Xi} = \omega^{-1}\mathbf{P}\mathbf{M}^{-1}\mathbf{C}\mathbf{P}^{+}, \tag{4a–e}$$

where $\Omega t = v\tau$ and $\tilde{\Omega} = \Omega/(v\omega)$. By setting $v > 1$, we may investigate subharmonic responses. Also note that the coupling of the variables is in terms of the arguments of the non-linear functions. This further economizes the procedure, since the Jacobian $\partial\mathbf{f}/\partial\mathbf{q}$ is now diagonal; it will be exploited later in section 3.1. The new system matrices for the reverse-idler gear pair are defined as

$$\mathbf{\Gamma} = \begin{bmatrix} \dfrac{K_1}{\omega^2}\left(\dfrac{R_A^2}{I_A} + \dfrac{R_B^2}{I_B}\right) & \dfrac{K_2 R_B^2}{I_B\omega^2} \\ \dfrac{K_1 R_B^2}{I_B\omega^2} & \dfrac{K_2}{\omega^2}\left(\dfrac{R_B^2}{I_B} + \dfrac{R_C^2}{I_C}\right) \end{bmatrix}, \qquad \mathbf{P} = \mathrm{diag}\,(\delta, \delta)^{-1}\begin{bmatrix} 1 & 1 & 0 \\ 0 & 1 & 1 \end{bmatrix}. \tag{5a, b}$$

A semi-definite 3-DOF system has thus been transformed into its equivalent 2-DOF definite system without sacrificing any dynamic or non-linear characteristics. The procedure is not to be confused with a dynamic reduction technique such as the Guyan reduction [19]. A simlar coupling was performed in reference [12], but a general coupling algorithm for arbitrary number of DOF was not presented therein. It should also be noted that this coupling is intended only for definite or semi-definite systems where the stiffness and damping elements occur in parallel. Note that although we have reduced the order of the physical system through coupling, we have also destroyed the symmetry of its

stiffness and damping matrices. In the above manner we have improved the computational speed and accuracy of the integration through coupling, yet often we are interested in predicting the *absolute* accelerations. These may be reconstructed with minimal additional computational effort through the utilization of an *anchoring* equation, which is presented in the dimensional form since it is not used in computations:

$$\ddot{\mathbf{z}} = \mathbf{M}^{-1}\mathbf{F} - \Omega v^{-1}\mathbf{M}^{-1}\mathbf{C}\mathbf{P}^{+}\mathbf{q}' - \mathbf{M}^{-1}\mathbf{K}\mathbf{P}^{+}\mathbf{f}(\mathbf{q}, \mathbf{q}'). \tag{6a}$$

Note that the time signals of the vector quantities on the right side of the equation are obtained from integration of the coupled system, equation (4a), while the system matrices in the above equation are preliminary values of those appearing in equations (4c–e). Usually, the anchoring equation at the end of the system branches (e.g., at inertias I_A or I_C in our system) are the simplest to implement since they involve fewer terms. An example is given below:

$$\ddot{\theta}_A = I_A^{-1}(T_{dc,A} - C_1 R_A \delta\Omega v^{-1} q_1' - K_1 R_A \delta f_1(q_1, q_1')). \tag{6b}$$

For small values of damping, the dynamic characteristics of the absolute acceleration, $\ddot{\theta}_A$, are mainly dictated by the non-linear force. It should be noted that the coupled variable formulation (4) is readily adapted to the rigid body kinematics approach used by Küçükay, Pfeiffer and other investigators [5–8] if the relation $q_i(\tau_+) = -rq_i(\tau_-)$ is used, where τ_+ is the time before impact, τ_- is the time after impact and r is the coefficient of restitution.

2.4. EFFECTIVE STIFFNESS CONCEPT

Due to very light torque loading in the neutral rattle-type problem, the gear teeth are free to "play" in the backlashes. Therefore, analysis or design procedures to solve gear rattle based on the full contact linear behavior [6, 9, 12] may be inappropriate. Yet we introduce the concept of effective stiffness in order to examine the non-linear aspects of the problem with the ease of linear analysis which may yield a *qualitative* understanding of the problem. In this context, the effective stiffness κ_i is the equivalent linearized stiffness of the non-linearity; i.e., $f_i(q_i, \dot{q}_i) \approx \kappa_i q_i$. For a gear backlash, κ_i is bounded by zero (no contact) and one (full contact), i.e., $0 \leqslant \kappa_i \leqslant 1$, where the in-between values correspond

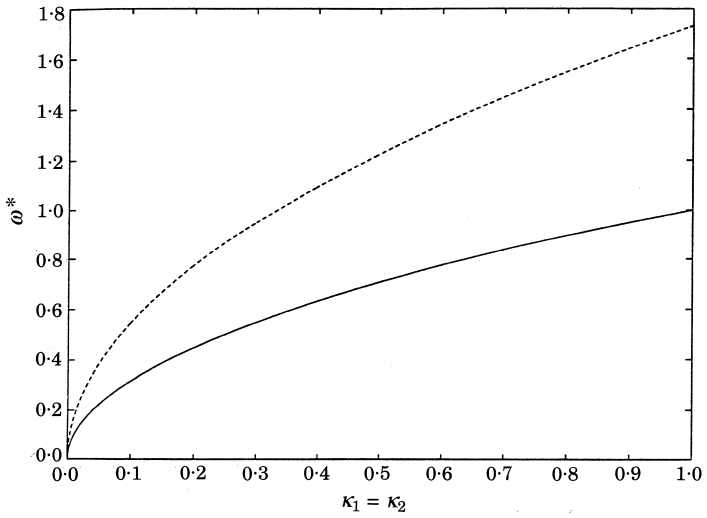

Figure 2. Variation of the natural frequencies of the linearized example with effective stiffness. ——, ω_1^*; - - - -, ω_2^*.

to the case in which the teeth are intermittently losing contact over a meshing cycle. The more often the teeth lose contact, the smaller is the effective stiffness, and therefore one may consider κ_i as an index of non-linearity. As shown in Figure 2, one may qualitatively see that the *effective* spacings between the natural frequencies of a linear system decrease as κ_i decreases. From this knowledge, we can anticipate that the spectral interactions will increase. This result will be confirmed later in section 4.

To calculate the effective stiffness, let us estimate the non-linear function $f_i(q_i, q_i')$ by the linear function $g_i(q_i)$. In order to minimize the ensuing error, $e_i = f_i(q_i, q_i') - g_i(q_i)$, in a least squares sense, the following equation must be satisfied:

$$\langle f_i(q_i, q_i')q_i \rangle = \langle g_i(q_i)q_i \rangle, \tag{7}$$

where $\langle\ \rangle$ is the expectation operator or time domain average, the frequency contents of which may be limited to suit the particular analysis. Since we are primarily interested in periodic solutions, we will assume only ergodic data in the subsequent analysis.

Now we utilize the fact that the approximation to the non-linearity must be linear if we plan to use it in the modal analysis. Accordingly, we let $g_i(q_i) = g_{dc,i} + g_{a,i} = \kappa_{dc,i}\langle q_i \rangle + \kappa_{a,i}(q_i - \langle q_i \rangle)$, which yields

$$\kappa_{dc,i} = \frac{\langle f_i(q_i, q_i') \rangle}{\langle q_i \rangle}, \qquad \kappa_{a,i} = \frac{\langle f_i(q_i, q_i')q_i \rangle - \langle f_i(q_i, q_i') \rangle \langle q_i \rangle}{\langle q_i^2 \rangle - \langle q_i \rangle^2}, \tag{8a, b}$$

which is equivalent to a stochastic linearization as presented by Wallaschek [20]. Such a linearization has the advantage that it preserves energy levels. Note that the effective stiffnesses are response variant, while for a linear system they are response invariant.

The second definition (8b) seems the best choice for the effective stiffness for use in modal analysis since if we use the approximation $g_{a,i} = \kappa_{a,i}q_{a,i}$ in equation (4a) with no damping or external excitation, we obtain the eigenvalue equation

$$(\mathbf{\Gamma K}_a - \tilde{\Omega}^2\mathbf{I})\mathbf{q}_a = \mathbf{0}, \qquad \mathbf{K}_a = \text{diag}\,(\kappa_{a,i}). \tag{9a, b}$$

Utilizing this knowledge, we can now establish the dependence of the effective natural frequencies upon the system response. Using equation (8b) with a single frequency response (which is equivalent to the describing function approach [11]) we consider two

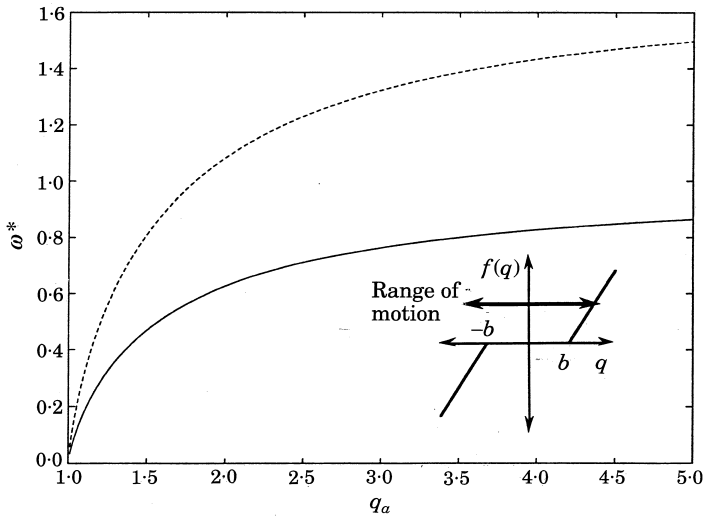

Figure 3. Variation of the natural frequencies of the system with response amplitude for a light mean load. ——, ω_1^*; - - - -, ω_2^*.

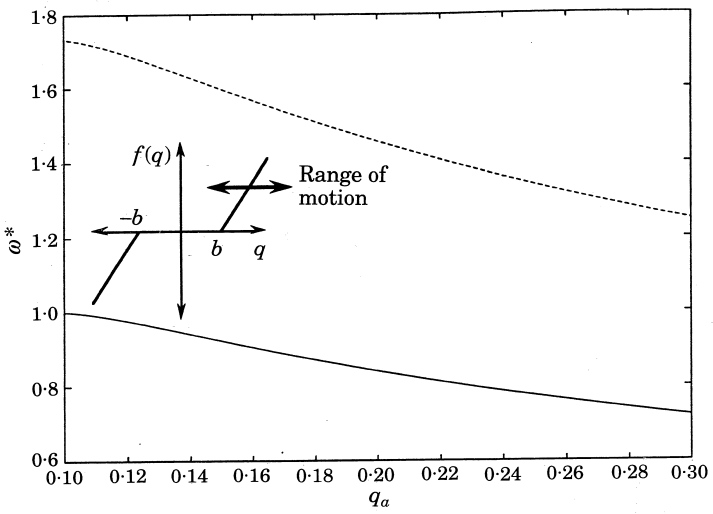

Figure 4. Variation of the natural frequencies of the system with response amplitude for a heavy mean load. ——, ω_1^*; - - - -, ω_2^*.

cases; (a) lightly loaded backlashes, and (b) heavily loaded backlashes. These are shown in Figures 3 and 4. In Figure 3, for low amplitude motion, the gear teeth start in the free play region of the backlashes and hence the effective natural frequencies are equal to zero (this corresponds to three uncoupled inertias). As the response increases, so does κ_i and consequently the effective natural frequencies and their spacings increase and eventually saturate at the linear values. In Figure 4, the gear teeth start out in full contact for small amplitude motion, but as the motion increases the gear teeth lose contact and hence κ_i and the effective natural frequencies drop.

The effective stiffnesses and natural frequencies were introduced in this study primarily as qualitative indicators of the contact conditions occurring in the meshes. They were used to show, for instance, that even well separated natural frequencies in the full contact regime can strongly interact with each other as contact diminishes. It should be pointed out that the effective stiffness concept (8a, b) is conceptually related to the procedures of obtaining non-linear modes [21]. Once the response dependent stiffnesses are obtained, the effective modes, as well as the natural frequencies, can be obtained via equation (9). Unlike reference [21], our results are based on the non-autonomous rather than autonomous responses. The dependence of natural frequencies upon system response at different mean loads was briefly examined by Munro [22], based on the mean stiffnesses of a linear time-varying, instead of a nonlinear time-invariant, system. Also, in the light of Pfeiffer's assertion [7] that mean quantities of the response are most important, viewing effective stiffnesses as an average amount of contact within the meshes can be useful. However, in formulations such as Pfeiffer's [5–8], the gears have no meshing compliance, so his model is incompatible with our concept of effective stiffnesses. The backbone curve arising from these effective natural frequencies also presents information about the impact conditions in the mesh, as will be shown in section 4.

3. NON-LINEAR AND STABILITY ANALYSIS

3.1. GALERKIN METHOD

While the single-term harmonic balance method (HBM), as in references [11, 12], was limited by tractability to a single non-linearity since the integrals are evaluated in closed

form, the numerical Galerkin treatment [23] containing multiple harmonics has no such limitation. Rather, the HBM is only a subset of the Galerkin method. The excitation and response of the system is assumed to be of the following form for the application of the Galerkin method:

$$\hat{\mathbf{Q}} = \mathscr{F}\hat{\mathbf{d}}, \qquad \hat{\mathbf{q}}^{(p)} = \mathscr{F}\mathscr{D}^{p}\hat{\mathbf{a}}, \qquad \hat{\mathbf{f}} = \mathscr{F}\hat{\mathbf{c}}, \tag{10a–c}$$

where

$$\hat{\mathbf{Q}} = [\mathbf{Q}(\tau_1), \ldots, \mathbf{Q}(\tau_m)]^{\mathrm{T}},$$

$$\hat{\mathbf{q}}^{(p)} = [\mathbf{q}^{(p)}(\tau_1), \ldots, \mathbf{q}^{(p)}(\tau_m)]^{\mathrm{T}}, \qquad \ldots, \qquad \hat{\mathbf{f}} = [\mathbf{f}(\tau_1), \ldots, \mathbf{f}(\tau_m)]^{\mathrm{T}},$$

$$\hat{\mathbf{d}} = [\mathbf{d}_0, \ldots, \mathbf{d}_{2n}]^{\mathrm{T}}, \qquad \hat{\mathbf{a}} = [\mathbf{a}_0, \ldots, \mathbf{a}_{2n}]^{\mathrm{T}}, \qquad \ldots, \qquad \hat{\mathbf{c}} = [\mathbf{c}_0, \ldots, \mathbf{c}_{2n}]^{\mathrm{T}}, \tag{10d–i}$$

and where the superscript (p) denotes the pth derivative with respect to τ, and where the discrete Fourier transform (DFT) matrices [24] are

$$\mathscr{F}_{j,1} = 1, \qquad \mathscr{F}_{j,2k} = \sin(k\tau_j), \qquad \mathscr{F}_{j,2k+1} = \cos(k\tau_j),$$

$$\mathscr{D}_{2k+1,2k} = -\mathscr{D}_{2k,2k+1} = k, \qquad j = 1, \ldots, m, \quad k = 1, \ldots, n, \quad m \geqslant 2n+1. \tag{10j, k}$$

Also, we must first define a residual which is to be minimized in some average sense [23]. In the time domain we have

$$\mathscr{R} = \mathbf{I}\mathbf{q}''(\tau) + \tilde{\Omega}^{-1}\mathbf{\Xi}\mathbf{q}'(\tau) + \tilde{\Omega}^{-2}\mathbf{\Gamma}\mathbf{f}(\mathbf{q}'(\tau), \mathbf{q}(\tau)) - \tilde{\Omega}^{-2}\mathbf{Q}(\tau) = \mathbf{0}, \tag{11a}$$

which holds for all values of time and thus may be considered the *strong form*. However, we are interested in the frequency domain and the transformed residual becomes

$$\mathscr{R} = ((\mathscr{D}^2 \otimes \mathbf{I}) + \tilde{\Omega}^{-1}(\mathscr{D}^1 \otimes \mathbf{\Xi}))\mathbf{a} + \tilde{\Omega}^{-2}(\mathscr{D}^0 \otimes \mathbf{\Gamma})\mathbf{c} - \tilde{\Omega}^{-2}\mathbf{d}, \tag{11b}$$

where $\mathbf{a} = \mathrm{vec}\,(\hat{\mathbf{a}}^{\mathrm{T}})$, etc [24, 25]. Since this residual is equivalent to the first in only an average sense, it may be considered the *weak form*. It should be noted that replacing the exact integrals of the Galerkin method [24, 26, 27] with their properly sampled discrete counterparts of the trigonometric functions as in equation (8b) constitutes an orthogonal collocation method [23].

Next we must employ Newton's method to solve the determining equations (11b) which necessitates the calculation of the Jacobian. The Newton's method for the coefficients takes the following form for the ith iteration:

$$^{(i+1)}\begin{Bmatrix}\mathbf{a}\\ \tilde{\Omega}\end{Bmatrix} = {}^{(i)}\begin{Bmatrix}\mathbf{a}\\ \tilde{\Omega}\end{Bmatrix} + {}^{(i)}\left[\frac{\partial\mathscr{R}}{\partial\mathbf{a}} \quad \frac{\partial\mathscr{R}}{\partial\tilde{\Omega}}\right]^{+}{}^{(i)}\mathscr{R} \tag{12a}$$

where the partial derivatives are given by

$$\frac{\partial\mathscr{R}}{\partial\mathbf{a}} = (\mathscr{D}^2 \otimes \mathbf{I}) + \tilde{\Omega}^{-1}(\mathscr{D}^1 \otimes \mathbf{\Xi}) + \tilde{\Omega}^{-2}(\mathscr{D}^0 \otimes \mathbf{\Gamma})(\mathscr{F}^{+} \otimes \mathbf{I})\mathscr{J}(\mathscr{F} \otimes \mathbf{I}),$$

$$\frac{\partial\mathscr{R}}{\partial\tilde{\Omega}} = 2\tilde{\Omega}^{-3}\mathbf{d} - \tilde{\Omega}^{-2}(\mathscr{D}^1 \otimes \mathbf{\Xi})\mathbf{a} - 2\tilde{\Omega}^{-3}(\mathscr{D}^0 \otimes \mathbf{\Gamma})\mathbf{c},$$

$$\mathscr{J} = \mathrm{diag}\left(\frac{\partial\mathbf{f}}{\partial\mathbf{q}}(\tau_1), \ldots, \frac{\partial\mathbf{f}}{\partial\mathbf{q}}(\tau_m)\right), \tag{12b–d}$$

and $\partial\mathbf{f}/\partial\mathbf{q}$ is itself a diagonal matrix for our case due to the use of the coupling procedure in section 2.3. One benefit of piecewise-linear systems is that at certain parameters the response is strictly linear (i.e., no impacts occur or $\kappa = 1$, $\forall\tau$) and these parameter values may be used as starting points for the Newton iteration. Such an example would be at high

frequencies and high mean loads (d.c.) where low amplitudes prevent impacts, or at very high alternating loads where the backlashes become saturated. Additionally, a continuation scheme may be implemented in conjunction with the Galerkin's method [28, 29] so that one may obtain the frequency response curves much the same way as with the HBM [11, 12]:

$$\begin{Bmatrix} \mathbf{a} \\ \tilde{\Omega} \end{Bmatrix} = \begin{Bmatrix} \mathbf{a} \\ \tilde{\Omega} \end{Bmatrix} + \mathbf{\Delta}, \qquad \mathbf{\Delta} = \mathscr{N} \begin{bmatrix} \partial \mathscr{R} / \partial \mathbf{a} & \partial \mathscr{R} / \partial \tilde{\Omega} \end{bmatrix}. \tag{13a, b}$$

Note that the independent parameter could also be chosen to be other system parameters such as the jth harmonic of the excitation on the ith DOF.

$$\frac{\partial \mathscr{R}}{\partial Q_{i,j}} = -\tilde{\Omega}^{-2} \frac{\partial \mathbf{d}}{\partial Q_{i,j}}. \tag{14}$$

Consequently, this term would replace $\partial \mathscr{R} / \partial \tilde{\Omega}$ (and $Q_{i,j}$ would replace $\tilde{\Omega}$) in the Newton and continuation equations (12) and (13).

For the sake of brevity in presentation, vector norms in the form of the root-mean-square (r.m.s.) displacement and velocity are presented, since the response may include many frequency components. These quantities may allow us to correlate results with measured noise data when available:

$$\tfrac{1}{2} q_{dc,i}^2 + q_{\text{r.m.s.},i}^2 = \tfrac{1}{2} (\mathbf{a}_{,i}^{\mathrm{T}} \mathscr{D}^0 \mathbf{a}_{,i}), \qquad q_{\text{r.m.s.},i}'^2 = \tfrac{1}{2} (\mathbf{a}_{,i}^{\mathrm{T}} \mathscr{D}^2 \mathbf{a}_{,i}), \tag{15a, b}$$

where the subscript, "i" denotes that only the ith DOF is considered. The convergence of the Galerkin method is based on the convergence of the r.m.s. displacement as well as the truncation error; e.g., $2n$ frequencies are used in the computations but only the first n frequencies are retained in equations (15a, b) [27]. Also, the effective stiffness of equation (8b) can be defined as

$$\kappa_{a,i} = (\mathbf{a}_{,i}^{\mathrm{T}} \mathbf{c}_{,i} - a_{0,i}^{\mathrm{T}} c_{0,i}) / (\mathbf{a}_{,i}^{\mathrm{T}} \mathbf{a}_{,i} - a_{0,i}^{\mathrm{T}} a_{0,i}), \tag{16}$$

which is obtained at no extra cost through the Galerkin method. As the repsonse changes, so will the effective stiffnesses and natural frequencies, unlike a linear system in which they are response invariant.

3.2. STABILITY ANALYSIS

The variational equation takes the following form

$$\Delta \mathbf{q}'(\tau) = \mathbf{A}(\tau) \Delta \mathbf{q}(\tau), \qquad \mathbf{A}(\tau) = \begin{bmatrix} \mathbf{0} & \mathbf{I} \\ -\partial \mathscr{R} / \partial \mathbf{q} & -\partial \mathscr{R} / \partial \mathbf{q}' \end{bmatrix}, \tag{17a, b}$$

when equation (11a) is implied and the matrix $\mathbf{A}(\tau)$ is the linearized state space matrix evaluated at the steady state solution. In order to determine the stability of a periodic system where $\mathbf{A}(\tau) = \mathbf{A}(\tau + T)$, Floquet theory [2, 4, 30, 31] is chosen, which yields the following set of differential equations which must be integrated from 0 to T:

$$\mathbf{\Phi}'(\tau) = \mathbf{A}(\tau) \mathbf{\Phi}(\tau), \qquad \mathbf{\Phi}(0) = \mathbf{I}. \tag{18}$$

Upon integrating the above equations, one obtains the *monodromy matrix* $\mathbf{\Phi}(T)$, the eigenvalues of which dictate the stability of the perturbations [30–32]. While period-doubling and secondary Hopf bifurcations have been observed for the example, saddle-node bifurcations have been more difficult to detect; what often appears to be a jump in the frequency response corresponds to a basin of attraction abruptly changing from a periodic attractor to a quasi-periodic or chaotic attractor.

Rather than directly integrating the variational equations (18), using the numerical algorithms as discussed in the next section, within the Galerkin method it is more convenient to calculate the monodromy matrix as follows for virtually no additional cost:

$$\mathbf{\Phi}(T) = \exp(2\pi\tilde{A}), \qquad \tilde{\mathbf{A}} = \begin{bmatrix} \mathbf{0} & \mathbf{I} \\ \tilde{\mathbf{A}}_1 & \tilde{\mathbf{A}}_2 \end{bmatrix},$$

$$\tilde{\mathbf{A}}_1 = -\tilde{\Omega}^{-2}\mathbf{\Gamma}\,\mathrm{diag}\,((I\otimes\mathscr{F}_1^+)\,\mathrm{vec}\,(\hat{\mathbf{f}}_q)),$$

$$\tilde{A}_2 = -\tilde{\Omega}^{-1}\mathbf{\Xi} - \tilde{\Omega}^{-2}\mathbf{\Gamma}\,\mathrm{diag}\,((\mathbf{I}\otimes\mathscr{F}_1^+)\,\mathrm{vec}\,(\hat{\mathbf{f}}_{q'})), \qquad \lambda_i = \exp(2\pi\lambda_i^*), \qquad (19a\text{–}e)$$

where $\mathscr{F}_1^+$ is the first row of $\mathscr{F}^+$ and λ^* is the eigenvalue of the time-averaged system $\tilde{\mathbf{A}}$, and where

$$\hat{\mathbf{f}}_q = [\mathbf{f}_q(\tau_1), \ldots, \mathbf{f}_q(\tau_m)]^{\mathrm{T}}, \qquad \mathbf{f}_q(\tau_k) = \left\{\frac{\partial f_1}{\partial q_1}(\tau_k), \ldots, \frac{\partial f_p}{\partial q_p}(\tau_k)\right\}^{\mathrm{T}}, \qquad (20f, g)$$

with similar expressions for $\hat{\mathbf{f}}_{q'}$ and $\mathbf{f}_{q'}(\tau_k)$. It is important to note that again the fact that our coupling yields a diagonal Jacobian has been exploited. These equations provide a crude estimate of the Floquet exponents while, if a more refined estimate is required, it may then be necessary to integrate equation (18) using numerical integration.

Yet another definition for the effective stiffness may be considered as the time-averaged stiffness and damping:

$$\kappa_{f1,i} = \left\langle \frac{\partial f_i}{\partial q_i}(q_i, q_i') \right\rangle, \qquad \kappa_{f2,i} = \left\langle \frac{\partial f_i}{\partial q_i'}(q_i, q_i') \right\rangle. \qquad (21a, b)$$

These definitions tie in neatly to the Floquet theory since they appear directly in the monodromy matrix (19), where equations (19c, d) could be rewritten as

$$\tilde{\mathbf{A}}_1 = -\tilde{\Omega}^{-2}\mathbf{\Gamma}\,\mathrm{diag}\,(\kappa_{f1,i}), \qquad \tilde{A}_2 = -\tilde{\Omega}^{-1}\mathbf{\Xi} - \tilde{\Omega}^{-2}\mathbf{\Gamma}\,\mathrm{diag}\,(\kappa_{f2,i}). \qquad (22a, b)$$

This definition of effective stiffness (21a, b) also corresponds to the average numerical "stiffness" of the system which is of interest with respect to numerical integration [18], as discussed in the next section.

3.3. NUMERICAL INTEGRATION

Due to the extremely non-linear nature of this problem, often one must resort to numerical integration in lieu of the semi-analytic methods previously discussed. This is especially true in the presence of phenomena such as the quasi-periodic or chaotic response. The fact that these responses are non-2π-periodic will cause the Galerkin method as we have currently formulated it to break down; a modified Galerkin method as proposed by Kundert [33] could handle quasi-periodic responses. For our problem the routine DOPRI5 was used; this algorithm is a modified Runge–Kutta method suggested by Dormand and Prince [34]. Note that classical (forward) numerical integration, unlike the Galerkin method, is incapable of tracking unstable and physically unrealizable solutions. Rather, if numerical integration in the form of shooting [30, 35, 36] is used, both the stable and unstable solutions may be tracked, as with the Galerkin method. Then the residual becomes the fixed point equation

$$\mathscr{R} = \mathscr{P}^1(\mathbf{u}_0) - \mathbf{u}_0, \qquad \mathbf{u}_0 = \{\mathbf{q}(0)^{\mathrm{T}} \quad \mathbf{q}'(0)^{\mathrm{T}}\}^{\mathrm{T}}, \qquad (23a, b)$$

where $\mathscr{P}^1$ represents the Poincaré mapping and, in the continuation procedure, $\mathbf{u}_0$ replaces $\mathbf{a}$ in equations (12a) and (13), and the Jacobian is obtained from equations (17) and (18) (see reference [36] for details). Shooting in its current form, like the presented Galerkin

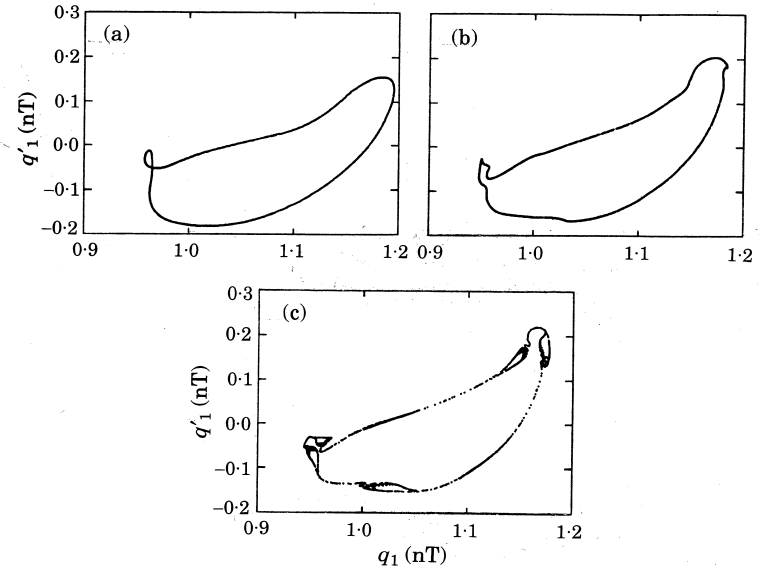

Figure 5. Poincaré maps for the system with $b_1 = b_2 = 1{\cdot}00$, $Q_{m,1} = Q_{m,2} = 0{\cdot}50$, $Q_{a,2} = 0{\cdot}00$, $\tilde{\Omega} = 1{\cdot}20$ and $\Delta\omega^* = 0{\cdot}73$. (a) $Q_{a,1} = 0{\cdot}2125$; (b) $Q_{a,1} = 0{\cdot}2250$; (c) $Q_{a,1} = 0{\cdot}2313$.

method, only searches for 2π-periodic solutions. Other authors have used modified shooting methods in order to trace quasi-periodic orbits [37].

A quasi-periodic response occurs much more often in the 2-DOF non-linear system than in the 1-DOF non-linear system [1, 12]. This is demonstrated in Figure 5, where using the Poincaré map one may observe how a quasi-periodic attractor (also called an *invariant*

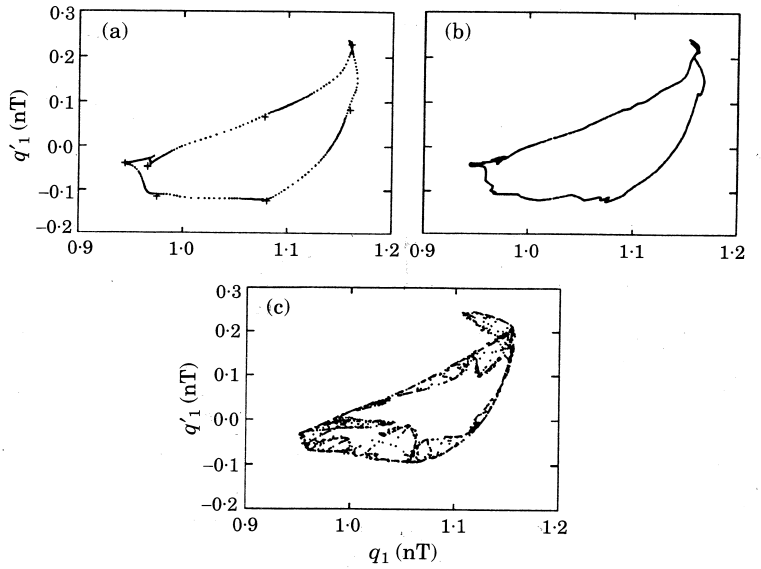

Figure 6. Poincaré maps for the system with $b_1 = b_2 = 1{\cdot}00$, $Q_{m,1} = Q_{m,2} = 0{\cdot}50$, $Q_{a,2} = 0{\cdot}00$, $\tilde{\Omega} = 1{\cdot}20$ and $\Delta\omega^* = 0{\cdot}73$. (a) $Q_{a,1} = 0{\cdot}2400$ (with fixed points from the seventh subharmonic denoted by $+$); (b) $Q_{a,1} = 0{\cdot}2413$; (c) $Q_{a,1} = 0{\cdot}2500$.

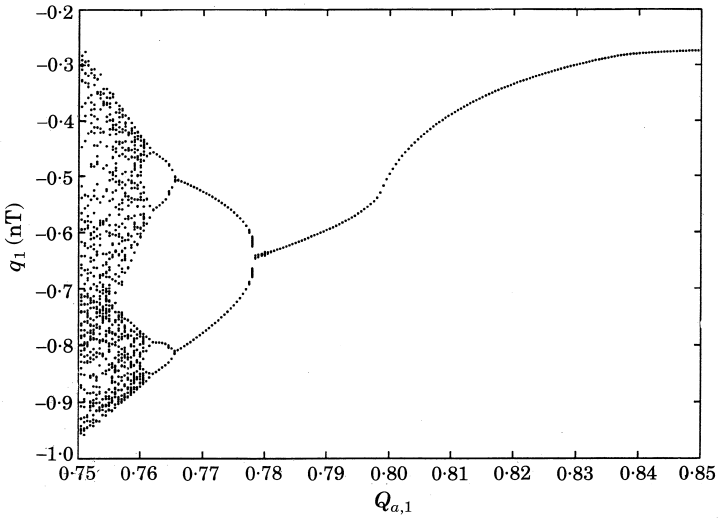

Figure 7. A bifurcation diagram of the system, given $b_1 = b_2 = 1{\cdot}00$, $Q_{m,1} = Q_{m,2} = 0{\cdot}50$, $Q_{a,2} = 0{\cdot}00$, $\tilde{\Omega} = 0{\cdot}20$ and $\Delta\omega^* = 0{\cdot}73$.

torus) breaks up into a chaotic attractor. In Figure 6, one can observe a quasi-periodic attractor evolve from a period-7 attractor (which in turn had evolved from another quasi-periodic attractor through phase-locking) and then further develop into a chaotic attractor. It should be noted that all this complex behavior occurred in a very small parameter span ($0{\cdot}21 \leqslant Q_{a,1} \leqslant 0{\cdot}25$).

Bifurcation diagrams using the Poincaré map [35, 38, 39] appear in Figures 7–9. In Figure 7 is illustrated an infinite cascade of period-doubling bifurcations which observes Feigenbaum's universal scaling [35, 38]. Feigenbaum's scaling applies to a scalar mapping [38], and with the symmetry in the response and backlashes in this case, such a mapping

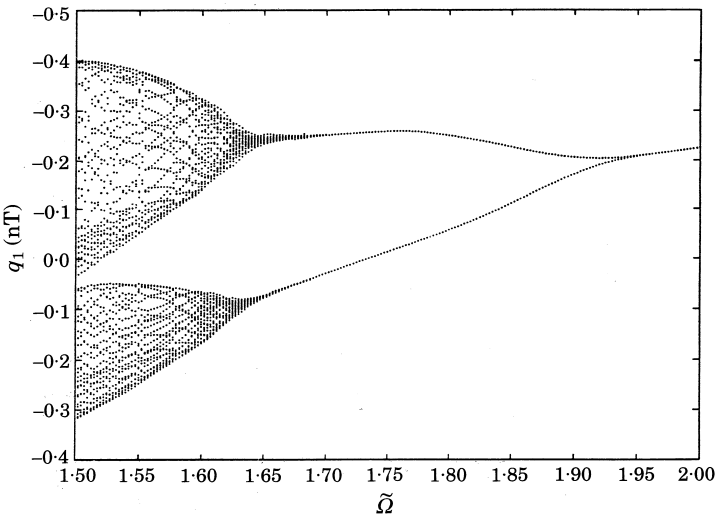

Figure 8. A bifurcation diagram of the system, given $b_1 = 0{\cdot}10$, $b_2 = 1{\cdot}00$, $Q_{m,1} = Q_{m,2} = 0{\cdot}50$, $Q_{a,1} = 0{\cdot}25$, $Q_{a,2} = 0{\cdot}00$ and $\Delta\omega^* = 0{\cdot}73$.

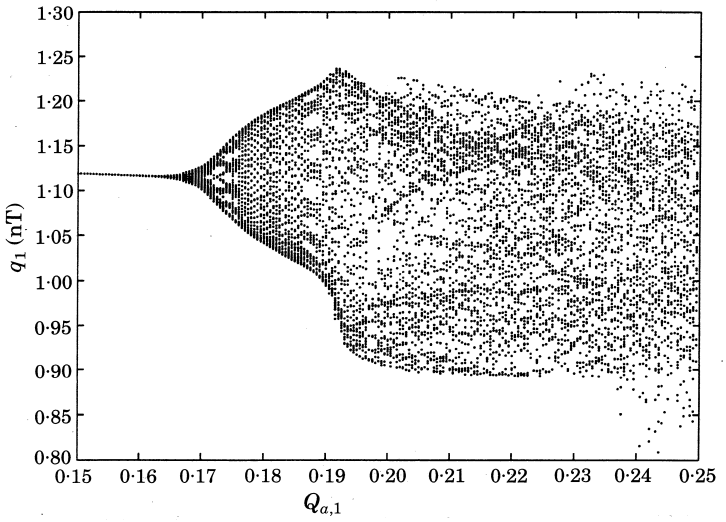

Figure 9. A bifurcation diagram of the system, given $b_1 = b_2 = 1{\cdot}00$, $Q_{m,1} = Q_{m,2} = 0{\cdot}50$, $Q_{a,2} = 0{\cdot}00$, $\tilde{\Omega} = 1{\cdot}20$ and $\Delta\omega^* = 0{\cdot}73$.

seems adequate. However, with the sufficient lack of symmetry in the case of Figure 8, the system cannot be reduced to such a mapping; the system is sufficiently complex to warrant a higher dimension mapping, and thus the bifurcation cascade shown here does not follow Feigenbaum's scaling. Figure 9 shows the full bifurcation sequence, of which certain instants were pictured in Figures 5 and 6. This figure confirms the presence of non-periodic responses over the parameter range considered. However, it should be pointed out that cataloguing all the branches is not the intention of this study. Rather, we are mostly interested in the periodic branches for the purpose of investigating spectral interaction and the variation of the natural frequencies.

4. SPECTRAL INTERACTION BETWEEN NON-LINEARITIES

In prior studies, the spectral interactions of a coupled oscillator has been investigated, but these models usually had either a single clearance non-linearity [1, 2, 12] or multiple analytic non-linearities [40, 41]. The only analytical study which contained multiple clearance type non-linearities required the assumption that the spectral interaction was negligible [11]. In view of the effective stiffness analysis of section 2.4, this assumption may not be valid. Consequently, we will investigate the spectral interactions between the two clearance non-linearities in the reverse-idler gear pair. Two cases selected to study spectral interactions are:

$$(1)\ \boldsymbol{\Gamma} = \begin{bmatrix} 2{\cdot}0 & 1{\cdot}0 \\ 1{\cdot}0 & 2{\cdot}0 \end{bmatrix}, \quad \Delta\omega^* = 0{\cdot}73; \qquad (2)\ \boldsymbol{\Gamma} = \begin{bmatrix} 2{\cdot}0 & 0{\cdot}5 \\ 0{\cdot}5 & 2{\cdot}0 \end{bmatrix}, \quad \Delta\omega^* = 0{\cdot}36.$$

Returning now to the concept of effective stiffness, we apply equation (8b) to the actual system response and trace the behavior of the effective natural frequencies. The dependence of the natural frequencies on the response amplitude is shown in Figures 10–15. One can see that for small amplitudes the response is linear and hence the natural frequencies coincide with their linear values of $\omega_1^* = 1$ and $\omega_2^* \approx 1{\cdot}732$ for case 1 and $\omega_1^* \approx 1{\cdot}225$ and $\omega_2^* \approx 1{\cdot}581$ for case 2. As the response becomes non-linear for larger amplitudes, the

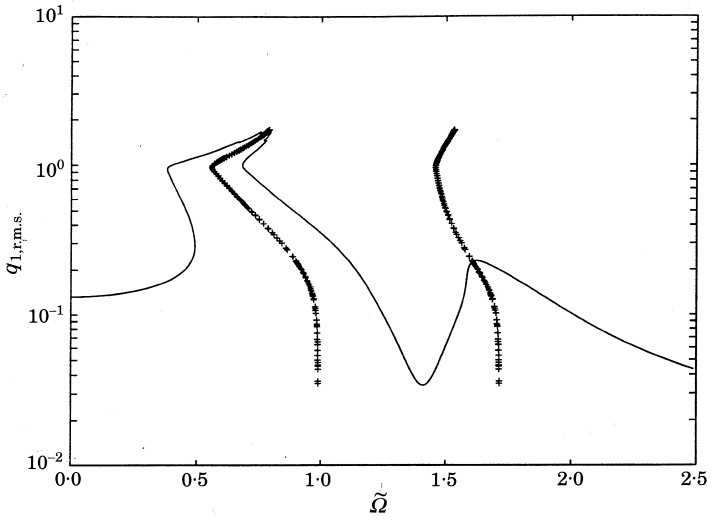

Figure 10. The frequency response of the system, showing the dependence of the natural frequencies on the response amplitude, given $b_1 = 1{\cdot}00$, $b_2 = 0{\cdot}00$, $Q_{m,1} = Q_{m,2} = 0{\cdot}50$, $Q_{a,1} = 0{\cdot}25$, $Q_{a,2} = 0{\cdot}00$ and $\Delta\omega^* = 0{\cdot}73$. ——, Response characteristics; +, backbone curve.

effective natural frequencies and their spacing decrease which implies increased spectral interaction.

In Figure 10, it is observed that when the second backlash is zero, the spectral interaction is mild, with the effective natural frequencies remaining distinct and well separated. The case of a single backlash was also presented in reference [12], and here it provides a benchmark to show the effect of including a second non-linearity. When the second backlash is increased, the effective natural frequencies shift lower and the interaction also

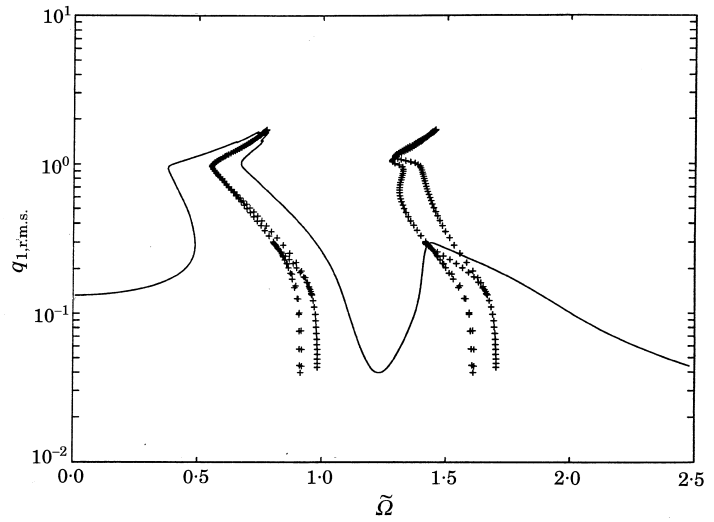

Figure 11. The frequency response of the system, showing the dependence of the natural frequencies on the response amplitude, given $b_1 = 1{\cdot}00$, $b_2 = 0{\cdot}10$, $Q_{m,1} = Q_{m,2} = 0{\cdot}50$, $Q_{a,1} = 0{\cdot}25$, $Q_{a,2} = 0{\cdot}00$ and $\Delta\omega^* = 0{\cdot}73$. ——, Response characteristics; +, backbone curve.

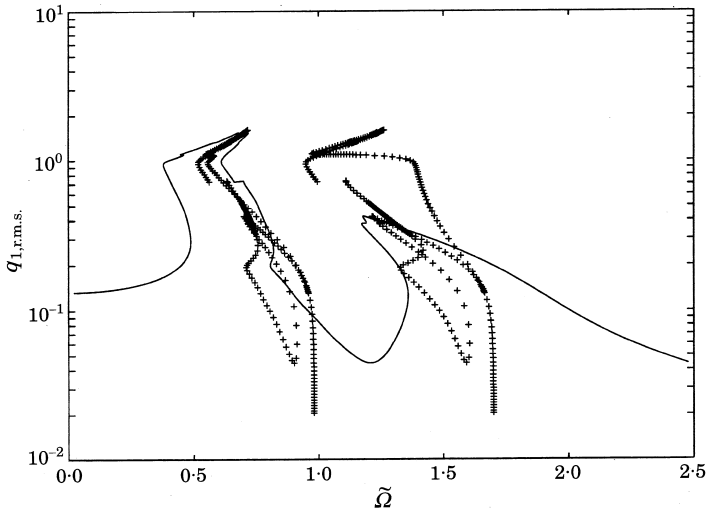

Figure 12. The frequency response of the system, showing the dependence of the natural frequencies on the response amplitude, given $b_1 = 1{\cdot}00$, $b_2 = 0{\cdot}50$, $Q_{m,1} = Q_{m,2} = 0{\cdot}50$, $Q_{a,1} = 0{\cdot}25$, $Q_{a,2} = 0{\cdot}00$ and $\Delta\omega^* = 0{\cdot}73$. ——, Response characteristics; +, backbone curve.

increases, as shown by Figure 11. In Figure 12, as the second backlash is further increased the two resonances begin to blend together, becoming nearly indistinguishable. This behavior could have been anticipated from our previous discussion of effective stiffnesses; as the effective stiffness in the second mesh decreases (with the increased backlash), the *effective* frequency spacing also decreases. Valuable information about the impact conditions in the meshes is revealed by the backbone curves. When the backbone is a vertical line, the response is linear (i.e., no impacts), while when the backbone veers to the left,

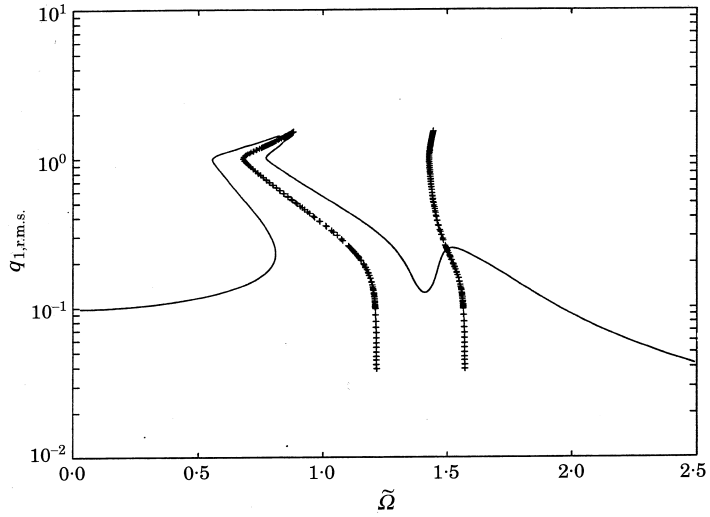

Figure 13. The frequency response of the system, showing the dependence of the natural frequencies on the response amplitude, given $b_1 = 1{\cdot}00$, $b_2 = 0{\cdot}00$, $Q_{m,1} = Q_{m,2} = 0{\cdot}50$, $Q_{a,1} = 0{\cdot}25$, $Q_{a,2} = 0{\cdot}00$ and $\Delta\omega^* = 0{\cdot}36$. ——, Response characteristics; +, backbone curve.

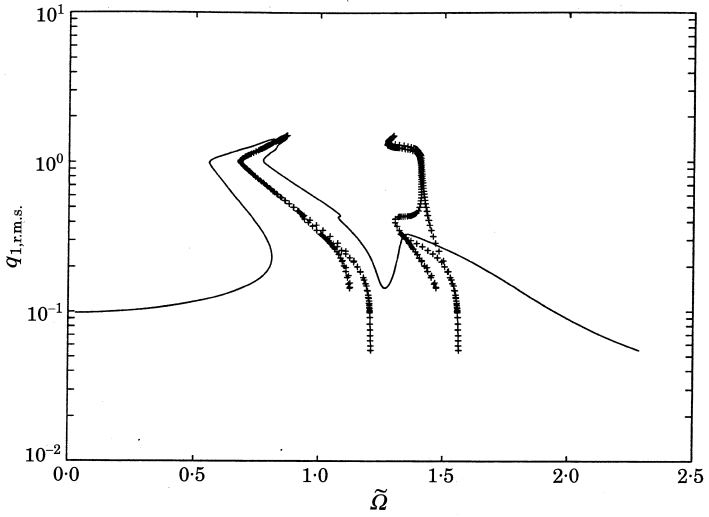

Figure 14. The frequency response of the system, showing the dependence of the natural frequencies on the response amplitude, given $b_1 = 1{\cdot}00$, $b_2 = 0{\cdot}10$, $Q_{m,1} = Q_{m,2} = 0{\cdot}50$, $Q_{a,1} = 0{\cdot}25$, $Q_{a,2} = 0{\cdot}00$ and $\Delta\omega^* = 0{\cdot}36$. ——, Response characteristics; +, backbone curve.

single-sided impacts are occurring in the mesh. This is due to a mean softening effect analogous to that in a Duffing's oscillator [40, 41]. As double-sided impacts occur, so does a mean hardening effect and, accordingly, the backbone shifts backs to the right. However due to the nature of backlashes, as the amplitudes further increase the backbone saturates to the linear natural frequency. One may observe that the backbone curves are not single-valued functions of the alternating or r.m.s. response; this is because the mean (d.c.) response varies also such that the impact conditions can be quite different for identical

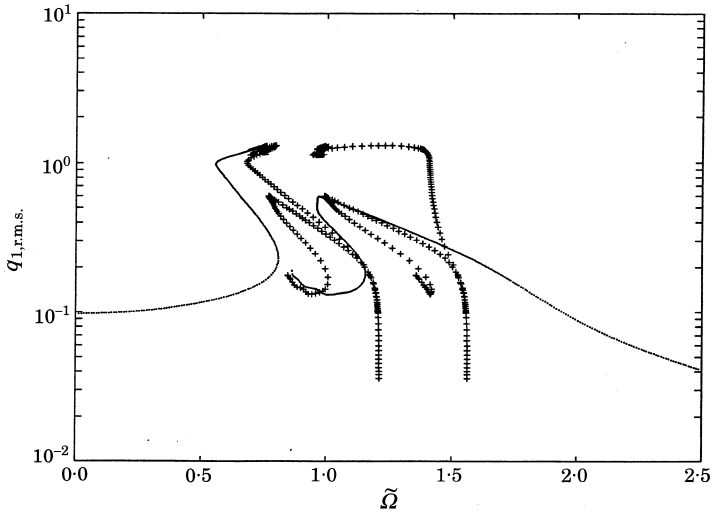

Figure 15. The frequency response of the system, showing the dependence of the natural frequencies on the response amplitude, given $b_1 = 1{\cdot}00$, $b_2 = 0{\cdot}50$, $Q_{m,1} = Q_{m,2} = 0{\cdot}50$, $Q_{a,1} = 0{\cdot}25$, $Q_{a,2} = 0{\cdot}00$ and $\Delta\omega^* = 0{\cdot}36$. ——, Response characteristics; +, backbone curve.

r.m.s. values. These phenomena are also displayed in Figures 13–15. In fact, due to the adjacent backlashes in the example, it is often difficult not to obtain high spectral interaction without heavily preloading one or both of the meshes.

For Figures 13–15, we have chosen case 2 from above and varied the second backlash as before in Figures 10–12. When the second backlash is zero (Figure 13), the spectral interaction is moderate in the linear regime, owing to the decrease in the linear natural frequency spacing from case 1. However, as the response becomes non-linear at larger amplitudes the effective frequency spacing appears to increase. As the second backlash is increased in Figures 14 and 15, one may observe that the spectral interaction increases as before. In fact, the resonances nearly overlap in Figure 15. Note that in the cases in which the second backlash is non-zero, in the vicinity of the anti-resonance the effective natural frequencies drop to values less than the linear natural frequencies since this is no longer a linear regime.

Also, from Figures 16 and 17 one may observe that in the middle to high frequency ranges the Galerkin method agrees reasonably with numerical integration, both classical

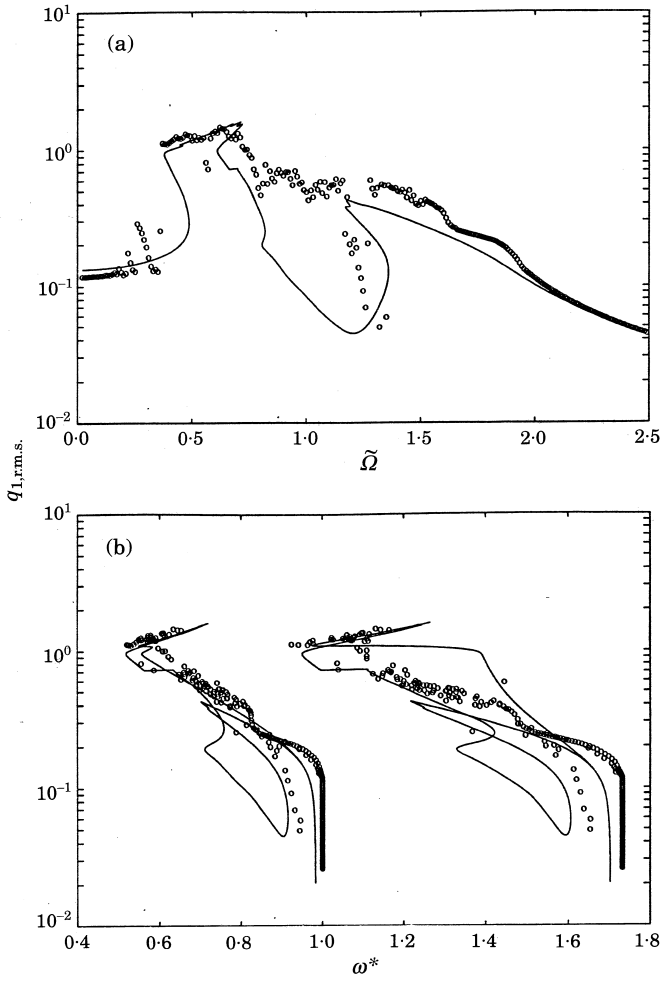

Figure 16. A comparison between the Galerkin method and classical numerical integration for the system, given $Q_{m,1} = Q_{m,2} = 0{\cdot}50$, $Q_{a,1} = 0{\cdot}25$, $Q_{a,2} = 0{\cdot}00$, $b_1 = 1{\cdot}00$ and $b_2 = 0{\cdot}50$. (a) Response characteristics; (b) backbone curve. ——, Galerkin method; ○, classical numerical integration.

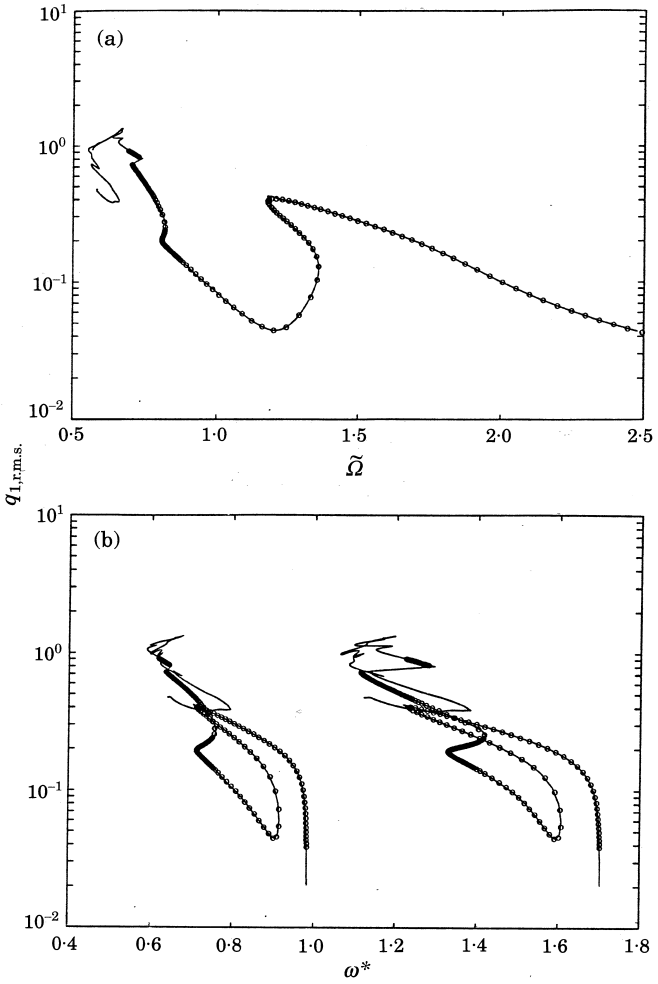

Figure 17. A comparison between the Galerkin method and the shooting method for the system, given $Q_{m,1} = Q_{m,2} = 0{\cdot}50$, $Q_{a,1} = 0{\cdot}25$, $Q_{a,2} = 0{\cdot}00$, $b_1 = 1{\cdot}00$ and $b_2 = 0{\cdot}50$. (a) Response characteristics; (b) backbone curve. ——, Galerkin method; ○, shooting method.

and shooting. However, for classical numerical integration, in the low frequency ranges or especially near the anti-resonance, the agreement is poor due to the dominance of quasi-periodic and chaotic responses in these regions. Both the Galerkin and shooting methods [36] as presented in this paper seem to be incapable of dealing with these responses. There are also some numerical difficulties at low frequencies which seem to be artifacts of the factors $\tilde{\Omega}^{-k}$ in the non-dimensionalization scheme.

5. CONCLUSIONS

This research has made contributions to the literature. Among these is the generalized method of coupling and scaling in order to reduce numerical difficulties faced in the simulation of the neutral rattle problem when two clearances are present concurrently. The Galerkin method was applied to a system with multiple clearances in order to investigate spectral interactions, while the previous investigators had largely studied single clearance

problems. Also included in the contributions is a concept of effective stiffness, which was developed to explain the complexities of spectral interactions in a non-linear system. It was shown that, in such a system, the resonance frequencies are indeed quite different from those predicted under full contact conditions. Furthermore, the effective stiffness concept was tied into the analytic procedures (Galerkin and Floquet methods). Unlike for a linear system, in which spectral interaction depends only on damping and the frequency spacings which are response invariant, in the non-linear system studied here the frequency spacing is response variant; hence the spectral interactions are dictated by both damping and effective stiffness. Further studies are expected to clarify this and other issues, especially when multiple non-linearities are excited by multiple excitations [36], in which case the necessity to track quasi-periodic solutions increases.

ACKNOWLEDGMENTS

We thank the Nissan Technical Center (Japan), the Center for Automotive Research at the Ohio State University, and the U.S. Army Research Office (URI Grant DAAL-03-92-G-0120; Project Monitor Dr T. L. Doligalski) for their financial support. Mr C. Padmanabhan is also acknowledged for introducing us to the shooting method [30], as well as for his insight into non-linear systems.

REFERENCES

1. A. Kahraman and R. Singh 1991 *Journal of Sound and Vibration* **144**, 469–506. Non-linear dynamics of a geared rotor–bearing system with multiple clearances.
2. Y. B. Kim and S. T. Noah 1990 *Nonlinear Dynamics* **1**, 221–241. Bifurcation analysis for a modified Jeffcott rotor with bearing clearances.
3. M. Kataoka, S. Ohno and T. Sugimoto 1991 *Japan Society of Mechanical Engineers*, *International Journal Series II* **34**, 345–354. A two-degree-of-freedom system including a clearance two-step hardening spring.
4. Y. B. Kim and S. T. Noah 1991 *Nonlinear Dynamics* **2**, 215–234. Response and bifurcation of a MDOF rotor system with a strong nonlinearity.
5. F. Küçükay 1984 *Proceedings of the Third International Conference on Vibrations in Rotating Machinery*, *Institution of Mechanical Engineers*, 81–90. Dynamic behavior of high speed gears.
6. F. Pfeiffer 1991 *Japan Society of Mechanical Engineers International Conference on Motion and Power Transmissions*, 43–48. Modelling problems of rattling in gear boxes.
7. K. Karagiannis and F. Pfeiffer 1991 *Nonlinear Dynamics* **2**, 367–387. Theoretical and experimental investigations of gear-rattling.
8. M. O. Hongler and L. Streit 1988 *Physica D* **29**, 402–408. On the origin of chaos in gearbox models.
9. A. Rust and F. K. Brandl 1990 *Proceedings of the XXIII FISITA Congress*. Definition, identification and elimination of obtrusive gear rattle noise.
10. R. Singh, H. Xie and R. J. Comparin 1989 *Journal of Sound and Vibration* **131**, 177–196. Analysis of an automotive neutral gear rattle.
11. R. J. Comparin and R. Singh 1990 *Transactions of the American Society of Mechanical Engineers*, *Journal of Mechanical Design* **112**, 237–245. An analytical study of automotive neutral gear rattle.
12. C. Padmanabhan and R. Singh 1992 *Journal of Sound and Vibration* **155**, 209–230. Spectral coupling issues in a two-degree-of-freedom system with clearance non-linearities.
13. T. Abe 1991 Personal communication and experimental data, Nissan Technical Center, Japan.
14. H. N. Özgüven and D. R. Houser 1988 *Journal of Sound and Vibration* **121**, 383–411. Mathematical models used in gear dynamics—a review.
15. G. W. Blankenship 1992 *Ph.D. Dissertation*, *The Ohio State University*. Analysis of force coupling and modulation phenomena in geared rotor systems.

16. K. H. Hunt and F. R. E. Crossley 1975 *Transactions of the American Society of Mechanical Engineers, Journal of Applied Mechanics* **42**, 440–445. Coefficient of restitution interpreted as damping in vibro-impact.
17. C. Padmanabhan, T. Rook and R. Singh 1992 *Proceedings of the Sixth International Power Transmission and Gearing Conference* **1**, 129–136. Computational issues associated with gear rattle analysis, part I: problem formulation.
18. R. Barlow, C. Padmanabhan and R. Singh 1992 *Proceedings of the Sixth International Power Transmission and Gearing Conference* **2**, 505–512. Computational issues associated with gear rattle analysis, part II: evaluation criterion for numerical algorithms.
19. R. D. Cooke, D. S. Malkus and M. E. Plesha 1989 *Concepts and Applications of Finite Element Analysis*. New York: John Wiley.
20. J. Wallaschek 1990 *International Journal of Non-linear Mechanics* **25**, 299–308. Dynamics of non-linear automobile shock-absorbers.
21. L. Jezequel and C. H. Lamarque 1991 *Journal of Sound and Vibration* **149**, 429–459. Analysis of non-linear dynamical systems by the normal form theory.
22. R. G. Munro 1962 *Doctoral Thesis, University of Cambridge*. The dynamic behavior of spur gears.
23. C. A. J. Fletcher 1984 *Computational Galerkin Methods*. New York: Springer-Verlag.
24. A. N. Jean and H. D. Nelson 1990 *Journal of Sound and Vibration* **143**, 473–489. Periodic response investigation of large order non-linear rotordynamic systems using collocation.
25. A. Graham 1981 *Kronecker Products and Matrix Calculus: With Applications*. New York: John Wiley.
26. M. Urabe and A. Reiter 1966 *Journal of Mathematical Analysis and Applications* **14**, 107–140. Numerical computation of non-linear forced oscillations by Galerkin's procedure.
27. E. L. Allgower and K. Georg 1990 *Numerical Continuation Methods: an introduction*. New York: Springer-Verlag.
28. F. H. Ling and X. X. Wu 1987 *International Journal of Non-linear Mechanics* **22**, 89–98. Fast Galerkin method and its application to determine periodic solutions of non-linear oscillators.
29. C. W. Wong, W. S. Zhang and S. L. Lau 1991 *Journal of Sound and Vibration* **149**, 91–105. Periodic forced vibration of unsymmetrical piecewise-linear systems by incremental harmonic balance method.
30. R. Seydel 1988 *From Equilibrium to Chaos: Practical Bifurcation and Stability Analysis*. New York: Elsevier.
31. G. Iooss and D. D. Joseph 1980 *Elementary Stability and Bifurcation Theory*. New York: Springer-Verlag.
32. P. Friedmann, C. E. Hammond and T. H. Woo 1977 *International Journal for Numerical Methods in Engineering* **11**, 1117–1136. Efficient numerical treatment of periodic systems with application to stability problems.
33. K. S. Kundert, G. B. Sorkin and A. Sangiovanni-Vincentelli 1988 *IEEE Transactions on Microwave Theory and Techniques* **36**, 366. Applying harmonic balance to almost-periodic circuits.
34. J. R. Dormand and P. J. Prince 1980 *Journal of Computational and Applied Mathematics* **6**(1), 19–26. A family of embedded Runge–Kutta formulae.
35. T. S. Parker and L. O. Chua 1989 *Practical Numerical Algorithms for Chaotic Systems*. New York: Springer-Verlag.
36. C. Padmanabhan 1995 accepted for publication in the *Journal of Sound and Vibration*. A parametric continuation technique for the analysis of periodically excited non-linear systems.
37. F. H. Ling 1991 *Journal of Sound and Vibration* **144**, 293–304. Quasi-periodic solutions calculated with the simple shooting technique.
38. J. M. T. Thompson and H. B. Stewart 1986 *Nonlinear Dynamics and Chaos*. New York: John Wiley.
39. I. A. Mahfouz and F. Badrakhan 1990 *Journal of Sound and Vibration* **143**, 289–328. Chaotic behavior of some piecewise-linear systems, part II: systems with clearance.
40. W. Stupnicka-Szemplińska 1990 *The Behavior of Nonlinear Vibrating Systems*, vol. II. New York: Elsevier.
41. J. Awrejcewicz and T. Someya 1991 *Journal of Sound and Vibration* **146**, 527–532. Periodic, quasi-periodic and chaotic orbits and their bifurcations in a system of coupled oscillators.

APPENDIX A: LIST OF SYMBOLS

a	Fourier coefficient of response
b	backlash breakpoint
c	Fourier coefficient of non-linearity
C	viscous damping
d	Fourier coefficient of excitation
$\mathscr{D}$	Fourier differentiation matrix
DOF	degrees of freedom
f	non-linear function
F	generalized absolute accelerations
$\mathscr{F}$	Fourier transform matrix (DFT)
g	linear functions
HBM	harmonic balance method
K	stiffness
M	mass, inertia
N	describing function
$\mathscr{N}$	null space operator
$\mathbf{P}$	transformation matrix
q	coupled displacement
Q	coupled forcing term
R	radius
t	time
T	external torque
$\mathbf{u}$	state space vector
z	generalized absolute displacement
Δ	correction or perturbation term
$\mathbf{\Gamma}$	non-dimensionalized stiffness matrix
$\mathbf{I}$	identity matrix
θ	angular displacement
Ω	excitation frequency
$\mathbf{\Xi}$	coupled damping matrix
$\mathbf{\Phi}$	monodromy (state transition) matrix
β	impact damping coefficient
δ	characteristic length
κ	effective stiffness
λ^*	eigenvalue
λ	Floquet exponent
τ	non-dimensionalized time
v	subharmonic index ($\geqslant 1$)
ω	characteristic frequency
ω^*	natural frequency
ζ	damping ratio

Subscripts

a	alternating component
d.c.	d.c. or mean component
r.m.s.	root-mean-square quantity

Superscripts

$(\,)'$	derivative with respect to τ
$(\dot{})$	derivative with respect to t
$(\hat{})$	row augmented form of vector, i.e. $\mathbf{a} = \text{vec}\,(\hat{\mathbf{a}}^{\mathrm{T}})$
$+$	Moore–Penrose pseudo-inverse

Operators and functions

diag	diagonal matrix operator [19]
vec	vector operator [19]